crystals

MDPI

Article

Synthesis, X-ray Structure, Hirshfeld Analysis of Biologically Active Mn(II) Pincer Complexes Based on *s*-Triazine Ligands

Saied M. Soliman [1,*], Hessa H. Al-Rasheed [2] and Ayman El-Faham [1,2,*]

[1] Department of Chemistry, Faculty of Science, Alexandria University, P.O. Box 426, Ibrahimia, Alexandria 21321, Egypt

[2] Department of Chemistry, College of Science, King Saud University, P.O. Box 2455, Riyadh 11451, Saudi Arabia; halbahli@ksu.edu.sa

* Correspondence: saied1soliman@yahoo.com or saeed.soliman@alexu.edu.eg (S.M.S.); aelfaham@ksu.edu.sa (A.E.-F.)

Received: 20 September 2020; Accepted: 12 October 2020; Published: 13 October 2020

Abstract: Herein, the synthesis and antimicrobial activities of [Mn($^{\mathbf{Morph}}$**BPT**)$(H_2O)_2NO_3$]NO_3; (**1**) and [Mn($^{\mathbf{Pip}}$**BPT**)$(H_2O)_2NO_3$]NO_3; (**2**) complexes of the pincer-type tridentate ligands $^{\mathbf{Morph}}$**BPT**; 4-(4,6-di(1*H*-pyrazol-1-yl)-1,3,5-triazin-2-yl)morpholine and $^{\mathbf{Pip}}$**BPT**; 2-(piperidin-1-yl)-4,6-di(1*H*-pyrazol-1-yl)-1,3,5-triazine are presented. Both complexes have slightly distorted octahedral coordination geometry. Their molecular packing depends on O–H···O, C–H···O hydrogen bonds and anion–π stacking contacts. Hirshfeld analysis was used to quantify the different contacts. Both complexes exhibited better anti-fungal activity than the standard Fluconazole and comparable antibacterial activity to Gentamycin against *Staphylococcus aureus* and *Escherichia coli* microbes. Moreover, complexes **1** and **2** are biologically more active than the free ligands against these microbes.

Keywords: Mn(II); antifungal; *s*-triazine; DFT; Hirshfeld

1. Introduction

The use of transition metal complexes as antimicrobial agents, and for their potential applications as inorganic pharmaceuticals and in medicine for diagnostics, has gained great interest from researchers [1–4]. In this regard, large and rising numbers of mono- and polynuclear complexes of different metals, and with different classes of chelating ligands involving Schiff bases, bipyridine, and phenanthroline with different anions, were presented in literature [5–14].

Of transition metals, manganese is considered an essential micronutrient in living organisms and has an important role in a broad range of enzyme-catalyzed reactions. There is no doubt about the potential use of Mn(II) complexes as catalytic scavengers for H_2O_2 against oxidative stress [7–15]. From this point of view, an increasing interest with the synthesis of more Mn(II) complexes in order to investigate their catalytic and antimicrobial activities. Mn(II) complexes of bipyridine and phenanthroline ligands were found to have promising antifungal activity comparable to the antifungal drug ketoconazole [15,16]. Mn(II) plays a key role in biology as required enzyme activator, which is responsible for metabolism and apoptosis [17,18]. In addition, a Mn(II) complex of the Schiff base ligand derived from 1,4-diaminobutane and pyridoxal hydrochloride showed a great anticancer activity against breast cancer [19]. More recently, a Mn(II) complex of a Schiff base derived from vitamin B6 was found as an apoptosis inducer in human MCF7 and HepG2 cancer cells [20].

In continuation to our interest with the *s*-triazine pincer complexes [21–24], and in light of the interesting recently reported data in literature [25–31], we are presenting here the synthesis of two new Mn(II) complexes with the *s*-triazine based *NNN*-pincer ligands shown in Figure 1. The structural

features of both complexes are elucidated. In addition, their antimicrobial activities as antibacterial and antifungal agents are presented.

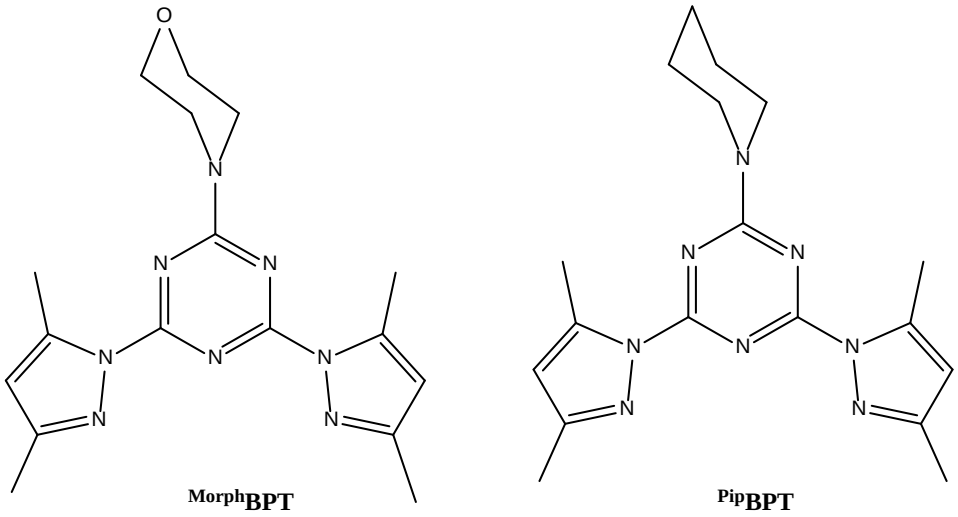

^{Morph}**BPT** ^{Pip}**BPT**

Figure 1. Structure of the pincer ligands [32].

2. Materials and Methods

Chemicals, reagents, and solvents used in this work were purchased from their commercial suppliers. The CHN analyses were determined using Perkin-Elmer 2400 instrument (PerkinElmer, Inc. 940 Winter Street, Waltham, MA, USA).

2.1. Preparation of the Organic Ligands

The organic ligands were prepared using the method reported in literature [32] (Supplementary data, Method S1, Figures S1 and S2).

*2.2. Syntheses of [Mn(^{Morph}**BPT**)$(H_2O)_2NO_3$]NO_3; (**1**) and [Mn(^{Pip}**BPT**)$(H_2O)_2NO_3$]NO_3; (**2**)*

In a 50 mL conical flask, the ligand solution (0.05 mmol) in 10 mL methanol was added to an aqueous solution of the $Mn(NO_3)_2{\cdot}4H_2O$ (~0.126 g, 0.05 mmol) in 10 mL water. The resulting clear solution was kept at room temperature for slow evaporation. Colorless crystals of the titled complexes were obtained after three days and were collected by filtration.

Yield:$C_{17}H_{26}MnN_{10}O_9$ (**1**) 80% with respect to the ligand. Anal. Calc. C, 35.86; H, 4.60; N, 24.60%. Found: C, 35.65; H, 4.52; N, 24.48%.

Yield; $C_{18}H_{28}MnN_{10}O_8$ (**2**) 77% with respect to the ligand. Anal. Calc. C, 38.10; H, 4.97; N, 24.69%. Found: C, 37.91; H, 4.91; N, 24.46%.

2.3. Crystal Structure Determination

The crystal structures of complexes **1** and **2** were determined by using a Bruker D8 Quest (Bruker Corporation, Massachusetts, MA, USA) diffractometer employing SHELXTL and SADABS programs [33–35]. Table 1 illustrated the refinement and crystal details. Hirshfeld calculations were performed using the default parameters of the Crystal Explorer 17.5 program [36–40].

2.4. Antimicrobial Studies

The bio-activities of the free ^{Morph}**BPT** and ^{Pip}**BPT** ligands, as well as the corresponding Mn(II) complexes against different microbes, were determined [32]. More details regarding the bio-experiments are found in Supplementary data.

Table 1. Crystal and refinement data of **1** and **2**.

Compound	1	2
Empirical formula	$C_{17}H_{26}MnN_{10}O_9$	$C_{18}H_{28}MnN_{10}O_8$
Formula weight (g/mol)	569.42	567.44
Temperature (K)	124(2)	117(2)
λ (Mo-Kα, Å)	0.71073	0.71073
Crystal system	Triclinic	Triclinic
Space group	P-1	P-1
Unit cell dimensions	a = 8.2794(5) Å	a = 7.830(5) Å
	b = 12.1167(7) Å	b = 12.951(7) Å
	c = 12.1738(7) Å	c = 13.990(7) Å
	α = 88.3660(19)°	α = 116.533(10)°
	β = 89.605(2)°	β = 94.832(14)°
	γ = 79.184(2)°	γ = 101.694(16)°
Volume ($Å^3$)	1199.08(12)	1217.9(12)
Z	2	2
Density (calc. g/cm^3)	1.577	1.547
Absorption coefficient (mm^{-1})	0.621	0.608
F(000)	590	590
Crystal size (mm^3)	0.29 × 0.21 × 0.11	0.31 × 0.23 × 0.19
θ range for data collection	2.36 to 26.34°	2.71 to 25.31°
Index ranges	−10 ≤ h ≤ 10, −15 ≤ k ≤ 15, −15 ≤ l ≤ 15	−9 ≤ h ≤ 9, −15 ≤ k ≤ 15, −16 ≤ l ≤ 16
Reflections collected	21,451	19,570
Independent reflections	4863 [R(int) = 0.0315]	4437 [R(int) = 0.0554]
Completeness to θ	99.30%	99.80%
Refinement method	Full-matrix least-squares on F^2	
Data/restraints/parameters	4863/0/385	4437/0/351
Goodness-of-fit on F^2	0.894	1.06
Final R indices [I>2sigma(I)]	R1 = 0.0275, wR2 = 0.0671	R1 = 0.0298, wR2 = 0.0732
R indices (all data)	R1 = 0.0341, wR2 = 0.0721	R1 = 0.0371, wR2 = 0.0775
Extinction coefficient	0.0100(8)	0.0157(17)
Largest diff. peak and hole	0.371 and −0.318	0.409 and −0.308
CCDC	2025609	2025610

2.5. Density Functional Theory (DFT) Calculations

Gaussian 09 (Wallingford, CT, USA) [41] built in MPW1PW91/TZVP method [42] were used for doing charge population [43] and atoms in molecules (AIM) [44] analyses, as previously described [2,21].

3. Results and Discussion

3.1. X-ray Crystal Structure Description

The structure with atomic numbering of [Mn($^{\mathbf{Morph}}$**BPT**)$(H_2O)_2NO_3$]NO_3 complex (**1**) are shown in Figure 2 and list of the most important geometric parameters are given in Table 2. It crystallized in the triclinic crystal system and P-1 space group, and Z = 2. This cationic complex has a hexa-coordinated Mn(II) with one tridentate pincer ligand, one monodentate nitrate ion, and two water molecules in its inner sphere while the outer sphere comprised two halves of nitrate ions. The manganese to nitrogen distance is significantly shorter with *s*-triazine (2.2170(14) Å) than the corresponding Mn–*N*(pyrazole) bonds (2.3187(15)–2.3269(14) Å). Moreover, the equatorial Mn–O bond is the shortest (2.1419(13) Å) where the length of the manganese to oxygen distances is in the order of Mn–O(equatorial water) < Mn–O(nitrate) < Mn–O(axial water). The two bite angles of the tridentate chelate are 69.49(5) and 69.09(5)° for N5–Mn1–N1 and N5–Mn1–N7, respectively while the angle between the two *trans* Mn–*N*(pyrazole) bonds is 138.55(5)° for N1–Mn1–N7. The O2–Mn1–O3 and O2–Mn1–O1 bond angles of these *cis* bonds are 90.33(5) and 80.66(6)°, respectively while the O3–Mn1–O1 *trans* bond angle is 167.72(5)°. The hexa-coordinated Mn(II) has a distorted octahedral configuration with a distorted square comprised the N1N5N7O2 atoms while the O1 and O3 atoms are located at the apexes. Using Shape 2.1 software (Barcelona, Spain), the continuous shape measure (CShM) values of 4.1 and 11.8 relative

to perfect octahedron and trigonal prism, respectively were computed. The CShM values revealed slightly distorted octahedral coordination geometry.

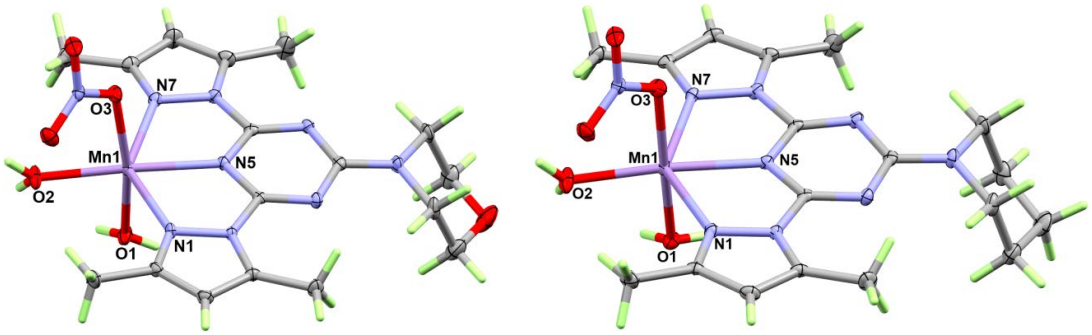

Figure 2. Structure and atomic numbering of the symmetric unit of **1** and **2**. Thermal ellipsoids were drawn at 50% probability level. Moreover, the nitrate counter ions were omitted for better clarity.

Table 2. The most important bond distances and angles of **1** and **2**.

Atoms	1	2
Mn1–O2	2.1416(12)	2.1288(19)
Mn1–O3	2.1683(11)	2.1604(16)
Mn1–O1	2.2159(12)	2.2306(17)
Mn1–N5	2.2172(12)	2.1973(18)
Mn1–N1	2.3188(13)	2.3097(19)
Mn1–N7	2.3267(13)	2.3580(18)
O2–Mn1–O3	90.35(5)	96.78(6)
O2–Mn1–O1	80.70(5)	83.33(6)
O3–Mn1–O1	167.76(5)	172.64(5)
O2–Mn1–N5	170.23(5)	166.35(6)
O3–Mn1–N5	97.55(4)	94.69(6)
O1–Mn1–N5	90.62(5)	84.34(6)
O2–Mn1–N1	115.16(5)	116.12(6)
O3–Mn1–N1	98.37(5)	94.40(6)
O1–Mn1–N1	93.02(5)	92.13(6)
N5–Mn1–N1	69.49(4)	70.18(5)
O2–Mn1-N7	106.03(5)	103.93(6)
O3–Mn1–N7	85.47(4)	86.40(6)
O1–Mn1–N7	88.98(5)	86.44(6)
N5–Mn1–N7	69.09(4)	69.39(5)
N1–Mn1–N7	138.55(4)	139.49(6)

The three dimensional structure of **1** is built by O–H···O hydrogen bonds and C–H···O interactions as shown in the left part of Figure 3. The donor-acceptor distances are generally shorter (2.662(3)–2.924(2) Å) in the former than in the latter (3.271(3)–3.455(3) Å) (Table 3). The packing of **1** is shown in the upper part of Figure 4. In addition, anion–π contacts play an important role in the packing of **1** (Figure S3 (Supplementary data) and Table 4).

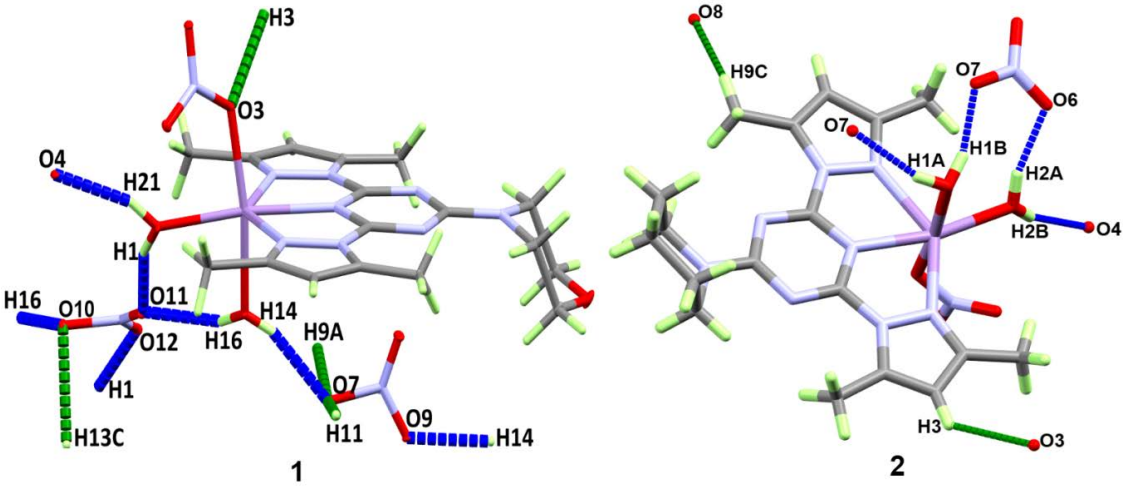

Figure 3. Important H–bond contacts in **1** and **2**. The green and blue colored contacts refer to the C–H···O and O–H···O interactions, respectively.

Table 3. The Geometric parameters of the H–bonds in **1** and **2**.

Atoms	D–H (Å)	H···A (Å)	D···A (Å)	D–H···A (°)
		1		
O2–H1···O11	0.82(2)	1.89(2)	2.662(3)	157(2)
O2–H1···O12	0.82(2)	1.95(2)	2.766(3)	175(2)
O1–H14···O9	0.83(2)	1.97(2)	2.728(3)	153(2)
O1–H14···O7^{i}	0.83(2)	1.96(2)	2.758(3)	161(2)
O1–H16···O10	0.85(2)	2.07(2)	2.884(3)	161(2)
O1–H16···O11	0.85(2)	2.07(2)	2.831(4)	150(2)
O2–H21···O5	0.85(2)	2.54(2)	2.924(2)	109(2)
O2–H21···O4^{ii}	0.85(2)	2.01(2)	2.816(2)	159(2)
C3–H3···O3^{iii}	0.95	2.52	3.319(2)	142
C9–H9A···O7^{iv}	0.98	2.49	3.455(3)	170
C11–H11···O7^{v}	0.95	2.39	3.328(3)	171
C13–H13C···O10	0.98	2.49	3.271(3)	136
Symmetry Code: (i) 1-x,1-y,2-z; (ii) -x,2-y,1-z; (iii) 1+x,y,z; (iv) -1+x,y,z; (v) -x,1-y,2-z				
		2		
O1–H1A···O7^{i}	0.83(3)	2.04(3)	2.839(3)	162(3)
O1–H1B···O7	0.86(2)	1.89(2)	2.723(3)	163(2)
O2–H2A···O6	0.87(2)	1.92(2)	2.758(3)	161(2)
O2–H2B···O4^{ii}	0.83(4)	1.99(4)	2.795(3)	162(4)
C3–H3···O3^{iii}	0.95	2.53	3.240(3)	132
C9–H9C···O8^{iv}	0.98	2.42	3.329(3)	154
Symmetry Code: (i) 1-x,1-y,-z; (ii) 1-x,1-y,1-z; (iii) 1+x,y,z; (iv) -x,1-y,-z				

Table 4. Anion–π contacts in complexes **1** and **2**.

1		**2**	
C7···O8^{i}	2.940(3)	C8···O7^{ii}	3.090(2)
N3···O8^{i}	3.077(3)	C7···O8^{ii}	2.982(2)
N4···O8^{i}	2.995(3)		
C8···O8^{i}	3.044(3)		
C6···O8^{i}	3.141(3)		
C6···O9^{i}	3.052(3)		
N5···O9^{i}	2.831(3)		
C8···O9^{i}	2.889(3)		
Symmetry Code: (i) x,y,z in **1** (ii) 1-x,1-y,-z in **2**			

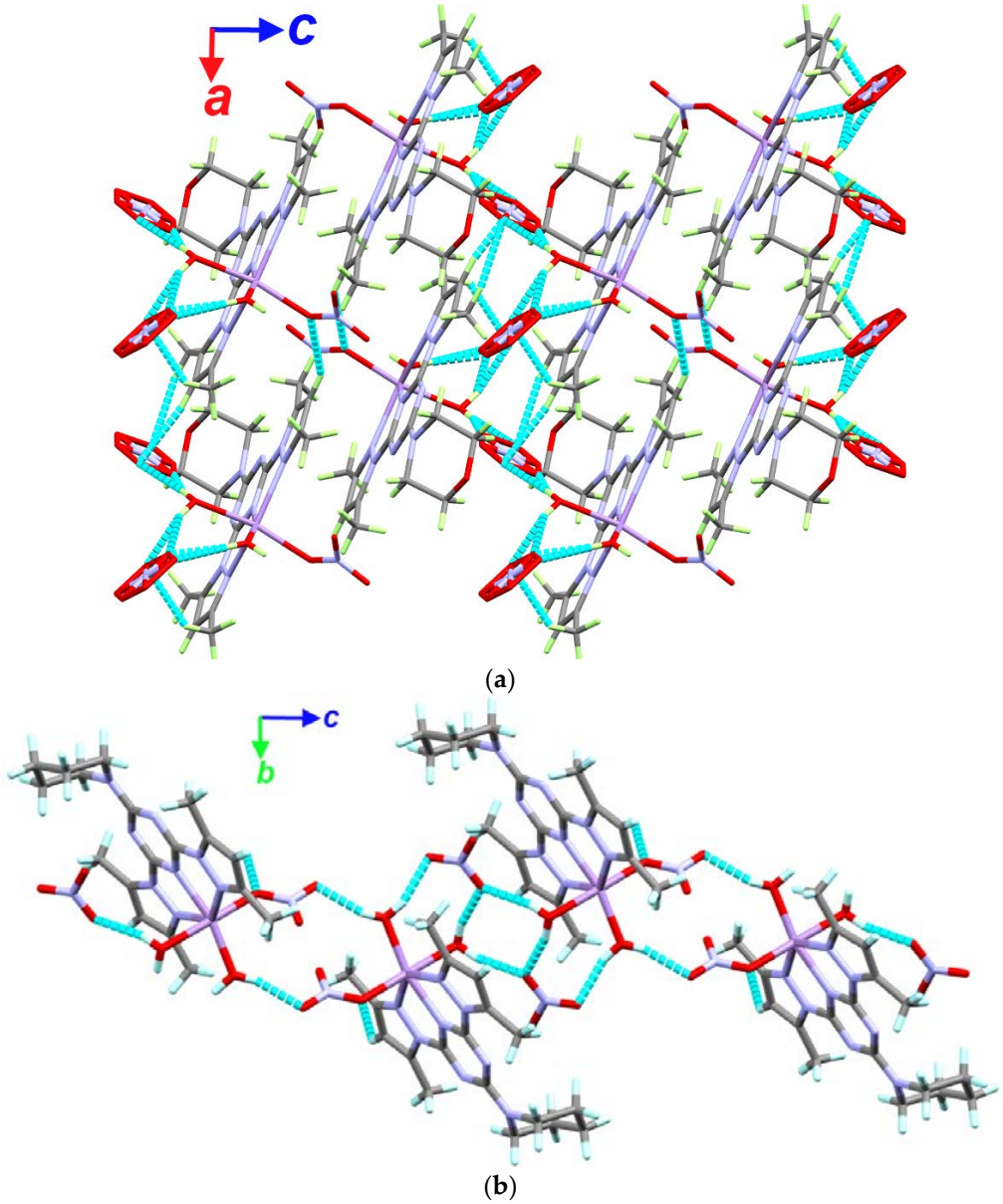

Figure 4. H–bond networks in **1** (**a**) and **2** (**b**).

The structure of [Mn(**^{Pip}BPT**)$(H_2O)_2NO_3$]NO_3 complex **2** is very similar to **1**. It also crystallized in the primitive triclinic unit cell with P-1 space group and two of the molecular formula per unit cell. In this case, the asymmetric unit comprised one cationic [Mn(**^{Pip}BPT**)$(H_2O)_2NO_3$] and one NO_3^- counter anion. In general, the Mn–N and Mn–O bonds are slightly shorter in this complex than those in **1** except one of the Mn–*N*(pyrazole) bonds as well as one Mn–O(water) bond, which is *trans* to the Mn–O(nitrate). The hexa-coordinated Mn(II) coordination configuration is slightly less distorted than that in **1** where the continuous shape measure values for **2** were computed to be 3.3 and 11.9 with respect to the perfect octahedron and trigonal prism, respectively. The most important O–H···O and C–H···O hydrogen bond contacts as well as the anion–π stacking contacts in **2** are shown in the right part of Figure 3 and Figure S3, respectively. The packing of **2** could be considered as 1D hydrogen bond polymer (Figure 4) while list of the hydrogen bonds is given in Table 3.

A slight structural difference between complexes **1** and **2** is the deviation of the Mn and coordinated equatorial oxygen atoms from the *s*-triazine plane. The plane passing through the perfectly planar aromatic *s*-triazine moiety is nearly passing through the center of Mn atom in complex **2** with only

0.040(2) Å deviation from this mean plane. The corresponding distances in complex **1** is 0.142(2) Å. The equatorial oxygen atom is deviated from this plane by a distance of 0.603(3) and 0.515(3) Å in complexes **1** and **2**, respectively. The reason could be simply attributed to the involvement of the *s*-triazine in larger number of anion–π stacking contacts in **1** compared to **2**.

There is another structural difference between complexes **1** and **2**. It is the orientation of the nitrate counter anion, with respect to the *s*-triazine moiety. In complex **1**, the nitrate anion is nearly perpendicular to the *s*-triazine mean plane where the angle between the two planes is 86.67(3)°. It seems that such situation allowed further anion–π stacking interactions in **1** compared to **2**. The corresponding angle between the two mean planes in complex **2** is only 26.64(3)°.

3.2. Analysis of Molecular Packing

Hirshfeld surfaces for **1** and **2** are given in Figure S4 (Supplementary data) while all possible contacts are shown in Figure 5. The decomposed d_{norm} maps of the short and most significant contacts are collected in Figure 6. The H···H, O···H, N···H and C···H interactions are the most frequent in both complexes. In complex **1**, these contacts contributed by 38.4, 37.5, 9.9 and 6.1%, respectively from the whole fingerprint area while the corresponding values in complex **2** are 45.2, 32.8, 8.8 and 5.2%, respectively. In addition, both complexes showed comparable amounts of anion–π stacking interactions with net C(*s*-triazine)···O(nitrate) and N(*s*-triazine)···O(nitrate) contacts of 2.8 and 2.5% for complexes **1** and **2**, respectively. The latter is weaker in complex **2** and not showed the characteristics of short contacts. The shortest C···O contact is C7···O8 (2.982(2) Å) in **2** while in **1** the shortest contact is C8···O9 (2.889(3) Å). Regarding the N···O contacts in complexes **1** and **2**, the shortest contact distances are N5···O9 (2.831(3) Å) and N6···O7 (3.077(2) Å), respectively. The N···O interaction in **2** is slightly longer than the vdW radii sum of nitrogen and oxygen indicating weaker interaction than **1**. The O···H contacts appeared strong in both complexes where the O11···H1 (1.742 Å) and O7···H1B (1.770 Å) are the shortest in complexes **1** and **2**, respectively. The values are different from those obtained from the CIF data given in Table 3 because in the Hirshfeld analysis the X–H (X = C, O) distances are normalized using the default criteria of Crystal Explorer 17.5 program. Many of the O···H contacts appeared as red regions in the d_{norm} map indicated shorter distance than the vdW radii sum of hydrogen and oxygen. In addition, complex **2** showed H···H and C–H···π interactions as red regions in the d_{norm} map with remarkable short distances of 1.959 Å (H5B···H5B) and 2.646 Å (C6···H5C). The latter occurred between the C–H of one methyl group from a complex unit with the *s*-triazine π-system from another complex unit. There are no observable π–π stacking interactions from the shape index and curvedness surfaces in both complexes.

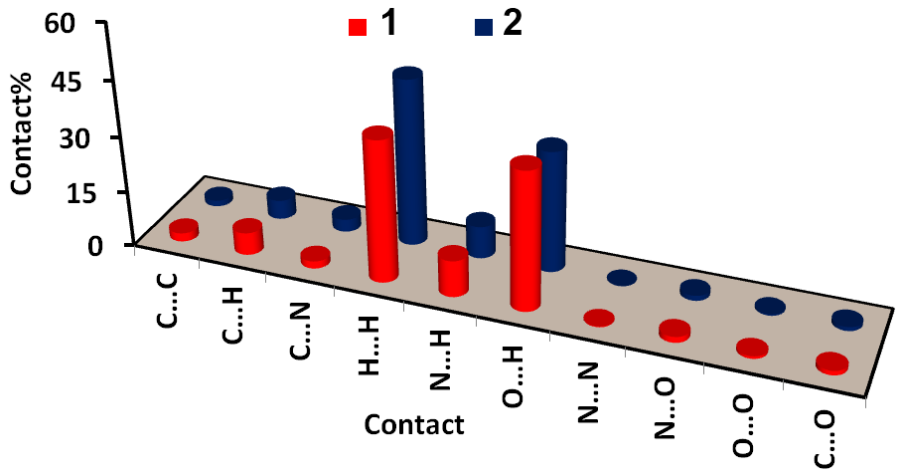

Figure 5. Summary of the intermolecular interactions in **1** and **2**.

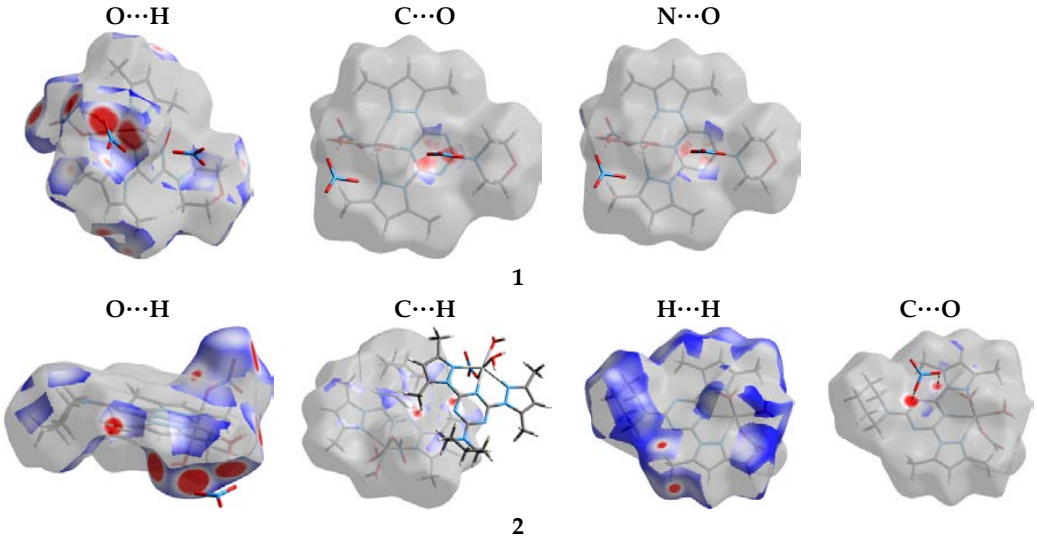

Figure 6. The d_{norm} maps of the most important contacts in **1** and **2**.

3.3. AIM Topology Analysis

The nature and strength of Mn–N and Mn–O interactions in the studied complexes were analyzed using atoms in molecules (AIM) calculations [44–54]. The electron density (ρ(r)) of the Mn–O and Mn–N bondings are in the range of 0.028–0.046 and 0.035–0.045 a.u, respectively which are generally lower than 0.1 a.u indicating weak interactions with closed shell characters (Table 5). With the exception of the Mn–N(*s*-triazine), the positive H(r) and V(r)/G(r) < 1 for the rest of Mn–N and Mn–O interactions are the typical characteristics of the closed shell interactions. The Mn–N(*s*-triazine) bonds have very slightly small negative H(r) values and V(r)/G(r) very slightly higher than one indicating that the Mn–N(*s*-triazine) bonds have higher covalent characters than the Mn–N(pyrazole). Among the Mn–O bonds, the equatorial bond which is located *trans* to the Mn–N(*s*-triazine) has the highest ρ(r) value and the highest interaction energy. As clearly seen in Figure 7, the Mn–O distances correlate well with the ρ(r) values as well as interaction energies (E_{int}). Similar observation could be noted for the Mn–N distances where the correlation coefficients (R^2) are found to be 0.992 and 0.993, respectively.

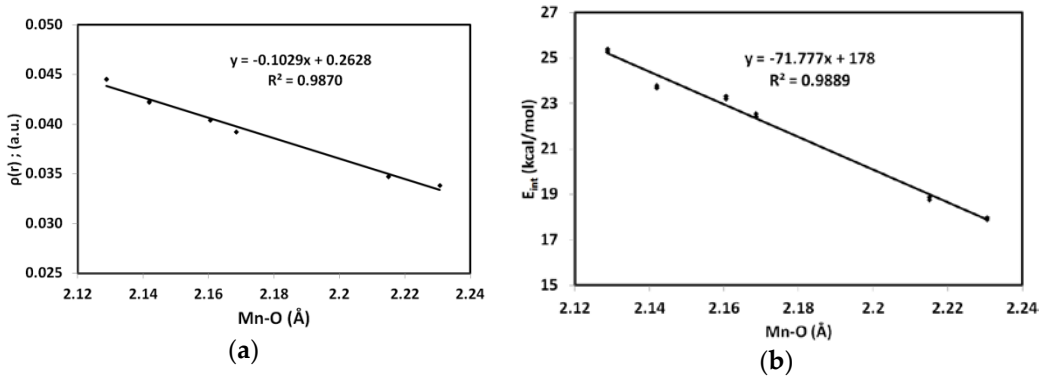

Figure 7. Correlation between ρ(r); (**a**) and interaction energies (E_{int}); (**b**) with Mn–O distances.

Table 5. Atoms in molecules (AIM) indices (a.u.) for the Mn–O and Mn–N bonds.

Bond	P(r)	G(r)	V(r)	E_{int} [a]	H(r) [b]	V(r)/G(r) [c]
			1 (MPW1PW91)			
Mn1–N1	0.0315	0.0526	−0.0511	16.0302	0.0015	0.9712
Mn1–N7	0.0310	0.0508	−0.0495	15.5195	0.0013	0.9737
Mn1–N5	0.0446	0.0730	−0.0749	23.5085	−0.0019	1.0257
Mn1–O1	0.0348	0.0617	−0.0602	18.8813	0.0015	0.9754
Mn1–O2	0.0423	0.0764	−0.0759	23.8078	0.0006	0.9927
Mn1–O3	0.0392	0.0731	−0.0719	22.5571	0.0012	0.9835
			1 (WB97XD)			
Mn1–N1	0.0315	0.0524	−0.0507	15.9153	0.0016	0.9689
Mn1–N7	0.0309	0.0506	−0.0491	15.4165	0.0014	0.9714
Mn1–N5	0.0445	0.0729	−0.0746	23.3928	−0.0017	1.0234
Mn1–O1	0.0347	0.0615	−0.0599	18.7798	0.0016	0.9734
Mn1–O2	0.0422	0.0763	−0.0755	23.6955	0.0007	0.9904
Mn1–O3	0.0392	0.0728	−0.0715	22.4445	0.0013	0.9820
			2 (MPW1PW91)			
Mn1–N1	0.0323	0.0536	−0.0522	16.3859	0.0014	0.9746
Mn1–N7	0.0285	0.0464	−0.0449	14.0784	0.0016	0.9662
Mn1–N5	0.0465	0.0774	−0.0796	24.9777	−0.0022	1.0283
Mn1–O1	0.0339	0.0592	−0.0574	17.9982	0.0018	0.9698
Mn1–O2	0.0446	0.0815	−0.0810	25.4111	0.0005	0.9940
Mn1–O3	0.0404	0.0754	−0.0743	23.3263	0.0010	0.9862
			2 (WB97XD)			
Mn1–N1	0.0323	0.0533	−0.0518	16.2604	0.0015	0.9724
Mn1–N7	0.0284	0.0462	−0.0445	13.9667	0.0017	0.9638
Mn1–N5	0.0464	0.0772	−0.0792	24.8540	−0.0020	1.0260
Mn1–O1	0.0338	0.0590	−0.0570	17.8993	0.0019	0.9676
Mn1–O2	0.0445	0.0812	−0.0806	25.2873	0.0006	0.9921
Mn1–O3	0.0404	0.0751	−0.0740	23.2066	0.0012	0.9846

[a] kcal/mol; [b] total energy density; [c] potential to kinetic energy density.

Bond orbital analysis (Table 6) of the Mn–N and Mn–O coordination interactions agreed very well with the experimental bond distances observed experimentally. It is clear that the bond order is the highest for Mn–N(*s*-triazine) compared to the Mn–N(pyrazole). Similarly, the equatorial Mn–O bond has the highest bond order compared to the rest of Mn–O bonds where the order of the Mn–O bond length is Mn–O(equatorial water) < Mn–O(nitrate) < Mn–O(axial water). The correlation coefficients of the Mn–N and Mn–O distances with the calculated bond order values are 0.996 and 0.976, respectively.

Table 6. Bond order analysis of the Mn–N and Mn–O coordination interactions.

Bond	MPW1PW91	WB97XD	MPW1PW91	WB97XD
	1		**2**	
Mn1–N1	0.143	0.144	0.142	0.143
Mn1–N7	0.136	0.137	0.122	0.123
Mn1–N5	0.198	0.199	0.206	0.207
Mn1–O1	0.129	0.129	0.119	0.119
Mn1–O2	0.163	0.163	0.170	0.171
Mn1–O3	0.157	0.158	0.159	0.161

Charge calculations of the free ligands allowed us to investigate the charge variations at the coordinating sites due to the chelation with the Mn(II) cation. It is obvious from the natural charges listed in Table 7 that all the coordinated donor atoms have more negative charge than those in the free ligand. The natural charge variation is higher (0.12–0.13 e) for the *s*-triazine *N*-site than the pyrazole (0.08–0.09 e) nitrogen atoms. As a conclusion, the coordination of the pincer ligand with the positively charged Mn(II) ion produced further polarization in the electron density towards the donor atom.

Table 7. The calculated natural charge at the *N*-sites of the free and coordinated pincer ligands using MPW1PW91(WB97XD) methods.

Atom	^{Morph}**BPT**	**1**	^{Pip}**BPT**	**2**
N5	−0.4618(−0.4740)	−0.5921(−0.6022)	−0.4671(−0.4794)	−0.5892(−0.5987)
N1	−0.2237(−0.2271)	−0.3163(−0.3191)	−0.2243(−0.2275)	−0.3042(−0.3069)
N7	−0.2015(−0.2275)	−0.3084(−0.3106)	−0.2224(−0.2256)	−0.3085(−0.3114)

3.4. Antimicrobial Activity

In the current study, the bio-activity of ^{Morph}**BPT** and ^{Pip}**BPT** as well as their Mn(II) complexes were tested as antibacterial and antifungal agents (Supplementary data, Method S2) [32,55–58]. The Mn(II) complexes showed good bio-activities against the target pathogenic microbes more than original ligand as illustrated from the inhibition zones (mm), which were measured as indicator for bioactivity of the tested compounds (Table 8) at concentration 200 μg/mL. ^{Morph}**BPT** is completely inactive against all tested microbes while ^{Pip}**BPT** showed good activity against *Staphylococcus aureus* and *Candida albicans*, while completely inactive against *Escherichia coli* (Table 8). Both Mn(II) complexes have better antibacterial and antifungal activity than the free ligands against *S. aureus*, *E. coli*, and *C. albicans*. Moreover, complexes **1** and **2** have better antifungal activity than the standard Fluconazole. In addition, the studied complexes have comparable antibacterial activity to Gentamycin against *S. aureus* and *E. coli*.

Table 8. Inhibition zones at 200 μg of the tested compounds by agar well diffusion method.

Compound	*S. aureus*	*E. coli*	*C. albicans*
^{Morph}**BPT**	-	-	-
^{Pip}**BPT**	11	-	12
1	21	17	15
2	27	20	17
Fluconazole	-	-	14
Gentamycin	28	21	-

The minimum inhibitory concentration (MIC) and minimum bactericidal concentration (MBC) values of all the tested complexes against *S. aureus*, *E. coli*, and *C. albicans* are reported (Table 9). It is clear that the studied Mn(II) complexes showed good bio-activity against *S. aureus* and *E. coli* as well as the fungus *C. albicans*. The MIC values are less for [Mn(^{Pip}**BPT**)$(H_2O)_2NO_3$]NO_3 than [Mn(^{Morph}**BPT**)$(H_2O)_2NO_3$]NO_3 against *S. aureus*, while both compounds showed similar antifungal actions against *C. albicans* and almost similar bio-activity against *E. coli*. Similarly, the MBC revealed these results very well.

Table 9. The minimum inhibitory concentration (MIC) and minimum bactericidal concentration (MBC) of complexes **1** and **2**.

Microbes	**1**		**2**	
	MIC (μg/mL)	MBC (μg/mL)	MIC (μg/mL)	MBC (μg/mL)
S. aureus	8.3	16.5	6.5	13.5
E. coli	8.3	16.5	8.3	16.8
C. albicans	18.5	100	18.5	100

4. Conclusions

[Mn(^{Morph}**BPT**)$(H_2O)_2NO_3$]NO_3; (**1**) and [Mn(^{Pip}**BPT**)$(H_2O)_2NO_3$]NO_3; (**2**) were synthesized using self-assembly of the pincer ^{Morph}**BPT** and ^{Pip}**BPT** ligands with $Mn(NO_3)_2{\cdot}4H_2O$ in water-alcohol mixture. The molecular and supramolecular structures of complexes **1** and **2** were investigated

using X-ray single crystal diffraction combined with Hirshfeld calculations. Their anti-microbial activities were compared with the free ligands and with Fluconazole and Gentamycin as standard agent. Both complexes showed better anti-fungal activity than the standard Fluconazole. Complexes **1** and **2** are biologically more active than the free ligands against *S. aureus*, *E. coli*, and *C. albicans* microbes.

Supplementary Materials: The following are available online at http://www.mdpi.com/2073-4352/10/10/931/s1. **Method S1**. General method for preparation of ligands. **Figure S1**. ^{1}H NMR and ^{13}C NMR of compound ligand ^{Morph}BPT. **Figure S2**. ^{1}H NMR and ^{13}C NMR of compound ligand ^{Pip}BPT. **Method S2**. Antimicrobial studies. **Figure S3**. Anion–π interactions in **1** and **2**. **Figure S4**. Hirshfeld surfaces mapped over d_{norm}, shape index and curvedness.

Author Contributions: Conceptualization, S.M.S.; formal analysis, S.M.S., H.H.A.-R. and A.E.-F.; funding acquisition, A.E.-F.; investigation, S.M.S. and H.H.A.-R.; resources, S.M.S. and A.E.-F.; software, S.M.S.; supervision, S.M.S.; writing—original draft, S.M.S., H.H.A.-R. and A.E.-F.; writing—review editing, S.M.S. All authors contributed to the first draft and the final version. All authors have read and agreed to the published version of the manuscript.

Funding: Deanship of Scientific Research, King Saud University, Saudi Arabia, grant number: RGP-1441-234.

Acknowledgments: The authors extend their thanks to the Deanship of Scientific Research at King Saud University for funding this work through research group no. (RGP-1441-234, Saudi Arabia).

Conflicts of Interest: The authors declare no conflict of interest.

References

1. Ronconi, L.; Sadler, P.J. Using coordination chemistry to design new medicines. *Coord. Chem. Rev.* **2007**, *251*, 1633–1648. [CrossRef]
2. Storr, T.; Thompson, K.H.; Orvi, C. Design of targeting ligands in medicinal inorganic chemistry. *Chem. Soc. Rev.* **2006**, *35*, 534–544. [CrossRef]
3. Biswas, B.; Kole, N.; Patra, M.; Shampa Dotta, S.; Ganguly, M. Synthesis, structural characterization and biological activity of a trinuclear zinc(II) complex: DNA interaction study and antimicrobial activity. *J. Chem. Sci.* **2013**, *125*, 1445–1453. [CrossRef]
4. Patel, M.N.; Joshi, H.N.; Patel, C.R. Cytotoxic, DNA binding, DNA cleavage and antibacterial studies of ruthenium–fluoroquinolone complexes. *J. Chem. Sci.* **2014**, *126*, 739–749. [CrossRef]
5. Madalan, A.M.; Kravtsov, V.C.; Pajic, D.; Zadro, K.; Simonov, Y.A.; Stanica, N.; Ouahab, L.; Lipkowski, J.; Andruh, M. Chemistry at the apical position of square-pyramidal copper(II) complexes: Synthesis, crystal structures, and magnetic properties of mononuclear Cu(II), and heteronuclear Cu(II)–Hg(II) and Cu(II)–Co(II) complexes containing $[Cu(AA)(BB)]^{+}$ moieties (AA = acetylacetonate, salicylaldehydate; BB = 1,10-phenanthroline, Me2bipy = 4,4′-dimethyl-2,2′-bipyridine). *Inorg. Chim. Acta* **2004**, *357*, 4151–4164.
6. Paulovicova, A.; El-Ayaan, U.; Fukuda, Y. Synthesis, characterization and X-ray crystal structures of two five-coordinate ternary copper(II) complexes containing acetylacetonate with 1,10-phenanthroline and 2,9-dimethyl phenanthroline. *Inorg. Chim. Acta* **2001**, *321*, 56–62. [CrossRef]
7. Triller, M.U.; Hsieh, W.Y.; Pecoraro, V.L.; Rompel, A.; Krebs, B. Preparation of Highly Efficient Manganese Catalase Mimics‖. *Inorg. Chem.* **2002**, *4*, 5544–5554. [CrossRef]
8. Wu, A.J.; Penner-Hahn, J.E.; Pecoraro, V.L. Structural, Spectroscopic, and Reactivity Models for the Manganese Catalases. *Chem. Rev.* **2004**, *104*, 903–938. [CrossRef]
9. Reddig, N.; Pursche, D.; Kloskowski, M.; Slinn, C.; Baldeau, S.M.; Rompel, A. Tuning the Catalase Activity of Dinuclear Manganese Complexes by Utilizing Different Substituted Tripodal Ligands. *Eur. J. Inorg. Chem.* **2004**, *2004*, 879–887. [CrossRef]
10. Signorella, S.; Rompel, A.; Buldt-Karentzopoulos, K.; Krebs, B.; Pecoraro, V.L.; Tuchagues, J.P. Reevaluation of the Kinetics of Polynuclear Mimics for Manganese Catalases. *Inorg. Chem.* **2007**, *46*, 10864–10868. [CrossRef]
11. Signorella, S.; Hureau, C. Bioinspired functional mimics of the manganese catalases. *Coord. Chem. Rev.* **2012**, *256*, 1229–1245. [CrossRef]
12. Biava, H.; Palopoli, C.; Duhayon, C.; Tuchagues, J.P.; Signorella, S. Synthesis, Structure, and Catalase-Like Activity of Dimanganese(III) Complexes of 1,5-Bis[(2-hydroxy-5-X-benzyl)(2-pyridylmethyl)amino] pentan-3-ol (X = H, Br, OCH_3). *Inorg. Chem.* **2009**, *48*, 3205–3214. [CrossRef] [PubMed]

13. Biju, A.R.; Rajasekharan, M.V. Structure, magnetic properties, catalase activity and DFT studies of $[Mn_2(\mu\text{-}RCOO)_2(\mu\text{-}OR)_2]^{2+}$ type dinuclear manganese(III,III) complexes. *Inorg. Chim. Acta* **2011**, *372*, 275–280. [CrossRef]
14. Vazquez-Fernandez, M.A.; Bermejo, M.R.; Fernandez-Garcia, M.I.; Gonzalez-Riopedre, G.; Rodriguez-Doutun, M.J.; Maneiro, M.J. Influence of the geometry around the manganese ion on the peroxidase and catalase activities of Mn(III)–Schiff base complexes. *Inorg. Biochem.* **2011**, *105*, 1538–1547. [CrossRef] [PubMed]
15. Kani, I.; Atlier, Ö.; Güven, K. Mn(II) complexes with bipyridine, phenanthroline and benzoic acid: Biological and catalase-like activity. *J. Chem. Sci.* **2016**, *128*, 523–536. [CrossRef]
16. Devereux, M.; McCann, M.; Leonl, V.; Geraghty, M.; McKee, V.; Wikaira, J. Synthesis and Biological Activity of Manganese (II) Complexes of Phthalic and Isophthalic Acid: X-Ray Crystal Structures of $[Mn(ph)(Phen)_2(H_2O)]$ $4H_2O$, $[Mn(Phen)_2(H_2O)_2]_2(Isoph)_2(Phen)$ $12H_2O$ and $\{[Mn(Isoph)(bipy)]_4{\cdot}2.75biby\}_n$($phH_2$ = Phthalic Acid; isoph = Isophthalic Acid; phen = 1,10-Phenanthroline; bipy = 2,2-Bipyridine). *Metal Based Drugs* **2000**, *7*, 275–288.
17. Avila, D.S.; Puntel, R.L.; Aschner, M. *Interrelations between Essential Metal Ions and Human Diseases*; Springer: Berlin, Germany, 2013; pp. 199–227.
18. Yoon, H.; Kim, D.S.; Lee, G.H.; Kim, K.W.; Kim, H.R.; Chae, H.J. Apoptosis Induced by Manganese on Neuronal SK-N-MC Cell Line: Endoplasmic Reticulum (ER) Stress and Mitochondria Dysfunction. *Environ. Health Toxicol.* **2011**, *26*, e2011017. [CrossRef]
19. Yadamani, S.; Neamati, A.; Homayouni-Tabrizi, M.; Beyramabadi, S.A.; Yadamani, S.; Gharib, A.; Morsali, A.; Khashi, M. Treatment of the breast cancer by using low frequency electromagnetic fields and Mn(II) complex of a Schiff base derived from the pyridoxal. *Breast* **2018**, *41*, 107–112. [CrossRef]
20. Tabatabayi, Z.S.; Tabrizi, M.H.; Neamati, A.; Beyramabadi, S.A. Mn(II) complex of a vitamin B6 Schiff base as an exclusive apoptosis inducer in human MCF7 and HepG2 cancer cells: Synthesis, characterization, and biological studies. *J. Cell. Biochem.* **2020**, *121*, 2677–2689. [CrossRef]
21. Soliman, S.M.; Almarhoon, Z.; El-Faham, A. Synthesis, Molecular and Supramolecular Structures of New Cd(II) Pincer-Type Complexes with s-Triazine Core Ligand. *Crystals* **2019**, *9*, 226. [CrossRef]
22. Soliman, S.M.; Elsilk, S.E.; El-Faham, A. Synthesis, structure and biological activity of zinc(II) pincer complexes with 2,4-*bis*(3,5-dimethyl-1*H*-pyrazol-1-yl)-6-methoxy-1,3,5-triazine. *Inorg. Chim. Acta* **2020**, *508*, 119627. [CrossRef]
23. Soliman, S.M.; Elsilk, S.E.; El-Faham, A. Syntheses, structure, Hirshfeld analysis and antimicrobial activity of four new Co(II) complexes with *s*-triazine-based pincer ligand. *Inorg. Chim. Acta* **2020**, *510*, 119753. [CrossRef]
24. Soliman, S.M.; Elsilk, S.E.; El-Faham, A. Novel one-dimensional polymeric Cu(II) complexes via Cu(II)-assisted hydrolysis of the 2,4-bis(3,5-dimethyl-1*H*-pyrazol-1-yl)-6-methoxy-1,3,5-triazine pincer ligand: Synthesis, structure, and antimicrobial activities. *Appl. Organometall. Chem.* **2020**, *510*, 119753.
25. Chen, W.; Chu, J.F.; Wang, Y.Q. Synthesis, characterization and preliminary reactivity behaviors with transitional metals of a new polydentate N-donor ligand. *J. Mol. Struct.* **2014**, *1068*, 237–244. [CrossRef]
26. Chu, J.F.; Zhang, M.Y.; Wang, Y.Q. Syntheses, Crystal Structures, and Properties of Three Copper(II) Complexes Constructed by 4-(4,6-Bis(1*H*-pyrazol-1-yl)-1,3,5-triazin-2-yl)morpholine. *Z. Anorg. Allg. Chem.* **2017**, *643*, 1101–1106. [CrossRef]
27. Aleksanyan, D.V.; Churusova, S.G.; Brunova, V.V.; Rybalkina, E.; Susova, O.; Peregudov, A.S.; Klemenkova, Z.S.; Denisov, G.L.; Kozlov, V.A. Synthesis, characterization, and cytotoxic activity of N -metallated rhenium(I) pincer complexes with (thio)phosphoryl pendant arms. *J. Organometall. Chem.* **2020**, *926*, 121498. [CrossRef]
28. Shakirova, J.R.; Hendi, Z.; Zhukovsky, D.D.; Sokolov, V.V.; Jamali, S.; Pavlovskiy, V.V.; Porsev, V.V.; Evarestov, R.A.; Tunik, S.P. NIR emitting platinum pincer complexes based on the N^N^C ligand containing {benz[4,5]imidazo[1,2-a]pyrazin} aromatic system; synthesis, characterization and photophysical study. *Inorg. Chim. Acta* **2020**, *511*, 119776. [CrossRef]
29. Fayoumi, A.; Lyubov, D.M.; Tolpygin, A.O.; Shavyrin, A.S.; Cherkasov, A.V.; Ob'edkov, A.M.; Trifonov, A.A. Sc and Y Hetero-alkyl Complexes with NCsp3N Pincer Type Diphenylmethanido Ligand: Synthesis, Structure and Reactivity. *Eur. J. Inorg. Chem.* **2020**, *2020*, 3259–3267. [CrossRef]

30. Gafurov, Z.N.; Bekmukhamedov, G.E.; Kagilev, A.A.; Kantyukov, A.O.; Sakhapov, I.F.; Mikhailov, I.K.; Khayarov, K.R.; Zaripov, R.B.; Islamov, D.R.; Usachev, K.S.; et al. Unsymmetrical pyrazole-based PCN pincer Ni(II) halides: Reactivity and catalytic activity in ethylene oligomerization. *J. Organometall. Chem.* **2020**, *912*, 121163. [CrossRef]
31. Safronov, S.V.; Gutsul, E.I.; Golub, I.E.; Dolgushin, F.M.; Nelubina, Y.V.; Filippov, O.A.; Epstein, L.M.; Peregudov, A.S.; Belkova, N.V.; Shubin, S.E. Synthesis, Structural Properties and Reactivity of Ruthenocene-based Pincer Pd(II) Tetrahydroborate. *Dalton Trans.* **2019**, *48*, 12720–12729. [CrossRef]
32. Sharma, A.; Ghabbour, H.; Khan, S.T.; de la Torre, B.G.; Albericio, F.; El-Faham, A. Novel pyrazolyl-s-triazine derivatives, molecular structure and antimicrobial activity. *J. Mol. Struct.* **2017**, *1145*, 244–253. [CrossRef]
33. Sheldrick, G.M. *Program for Empirical Absorption Correction of Area Detector Data*; University of Göttingen: Göttingen, Germany, 1996.
34. Sheldrick, G.M. SHELXT-Integrated space-group and crystal-structure determination. *Acta Cryst. A* **2015**, *71*, 3–8. [CrossRef] [PubMed]
35. Spek, A.L. Structure validation in chemical crystallography. *Acta Cryst. D* **2009**, *65*, 148–155. [CrossRef] [PubMed]
36. Turner, M.J.; McKinnon, J.J.; Wolff, S.K.; Grimwood, D.J.; Spackman, P.R.; Jayatilaka, D.; Spackman, M.A. *Crystal Explorer 17*; University of Western Australia: Perth, Australia, 2017. Available online: http://hirshfeldsurface.net (accessed on 12 June 2017).
37. Spackman, M.A.; Jayatilaka, D. Hirshfeld surface analysis. *Cryst. Eng. Comm.* **2009**, *11*, 19–32. [CrossRef]
38. Spackman, M.A.; McKinnon, J.J. Fingerprinting intermolecular interactions in molecular crystals. *Cryst. Eng. Commun.* **2002**, *4*, 378–392. [CrossRef]
39. Bernstein, J.; Davis, R.E.; Shimoni, L.; Chang, N.-L. Patterns in hydrogen bonding: Functionality and graph set analysis in crystals. *Angew. Chem. Int. Ed. Engl.* **1995**, *34*, 1555–1573. [CrossRef]
40. McKinnon, J.J.; Jayatilaka, D.; Spackman, M.A. Towards quantitative analysis of intermolecular interactions with Hirshfeld surfaces. *Chem. Commun.* **2007**, *37*, 3814–3816. [CrossRef]
41. Frisch, M.J.; Trucks, G.W.; Schlegel, H.B.; Scuseria, G.E.; Robb, M.A.; Cheeseman, J.R.; Scalmani, G.; Barone, V.; Mennucci, B.; Petersson, G.A.; et al. *GAUSSIAN 09.Revision A02*; Gaussian Inc.: Wallingford, CT, USA, 2009.
42. Adamo, C.; Barone, V. Exchange functionals with improved long-range behavior and adiabatic connection methods without adjustable parameters: The mPWmPW and mPW1PWmPW1PW models. *J. Chem. Phys.* **1998**, *108*, 664–675. [CrossRef]
43. Glendening, E.D.; Reed, A.E.; Carpenter, J.E.; Weinhold, F. *NBO Version 3.1, CI*; University of Wisconsin: Madison, WI, USA, 1998.
44. Lu, T.; Chen, F. Multiwfn: A multifunctional wavefunction analyzer. *J. Comput. Chem.* **2012**, *33*, 580–592. [CrossRef]
45. Bader, R.F.W. *Atoms in Molecules: A Quantum Theory*; Oxford University Press: Oxford, UK, 1990.
46. Matta, C.F.; Hernandez-Trujillo, J.; Tang, T.-H.; Bader, R.F.W. Hydrogen-hydrogen bonding: A stabilizing interaction in molecules and crystals. *Chem. Eur. J.* **2003**, *9*, 1940–1951. [CrossRef]
47. Grabowski, S.J.; Pfitzner, A.; Zabel, M.; Dubis, A.T.; Palusiak, M. Intramolecular H–H interactions for the Crystal Structures of [4-((*E*)-But-1-enyl)-2,6-dimethoxyphenyl]pyridine-3-carboxylate and [4-((*E*)-Pent-1-enyl)-2,6-dimethoxyphenyl]pyridine-3-carboxylate; DFT calculations on modeled styrene derivatives. *J. Phys. Chem. B* **2004**, *108*, 1831–1837. [CrossRef]
48. Matta, C.F.; Castillo, N.; Boyd, R.J. Characterization of a closed-shell fluorine-fluorine bonding interaction in aromatic compounds on the basis of the electron density. *J. Phys. Chem. A* **2005**, *109*, 3669–3681. [CrossRef] [PubMed]
49. Pendás, A.M.; Francisco, E.; Blanco, M.A.; Gatti, C. Bond paths as privileged exchange channels. *Chem. Eur. J.* **2007**, *13*, 9362–9371. [CrossRef] [PubMed]
50. Bobrov, M.F.; Popova, G.V.; Tsirelson, V.G. A topological analysis of electron density and chemical bonding in cyclophosphazenes $P_nN_nX_{2n}$ (X = H, F, Cl; n = 2, 3, 4). *Russ. J. Phys. Chem.* **2006**, *80*, 584–590. [CrossRef]
51. Gatti, C. Chemical bonding in crystals: New directions. *Zeitschrift für Kristallographie* **2005**, *220*, 399–457. [CrossRef]
52. Gibbs, G.V.; Downs, R.T.; Cox, D.F.; Ross, N.L.; Boisen, M.B., Jr.; Rosso, K.M. Shared and closed-shell O-O interactions in silicates. *J. Phys. Chem. A* **2008**, *112*, 3693–3699. [CrossRef] [PubMed]
53. Espinosa, E.; Molins, E.; Lecomte, C. Hydrogen bond strengths revealed by topological analyses of experimentally observed electron densities. *Chem. Phys. Lett.* **1998**, *285*, 170–173. [CrossRef]

54. Cremer, D.; Kraka, E. Chemical Bonds without Bonding Electron Density—Does the Difference Electron-Density Analysis Suffice for a Description of the Chemical Bond? *Angew. Chem. Int. Ed. Engl.* **1984**, *23*, 627–628. [CrossRef]
55. De Souza, S.M.; Delle Monache, F.; Smânia, A. Antibacterial activity of coumarins. *Zeitschrift fuer Naturforschung C* **2005**, *60*, 693–700. [CrossRef]
56. Arshad, M.; Bhat, A.R.; Hoi, K.K.; Choi, I.; Athar, F. Synthesis, characterization and antibacterial screening of some novel 1,2,4-triazine derivatives. *Chin. Chem. Lett.* **2017**, *28*, 1559–1565. [CrossRef]
57. Torshizi, H.M.; Jahromi, S.Z. Synthesis, Characterization and in Vitro Antimicrobial Screening of the Xanthate Derivatives and their Iron(II) Complexes. *Iran. J. Chem. Chem. Eng.* **2017**, *36*, 43–54.
58. Dhokale, N.T.; Karale, B.K.; Nagawadw, A.V. Synthesis, Characterization and Antibacterial Studies on Mn(II) and Fe(II) Complexes of N, O Donor Salicyloyl Pyrazole Oxime Schiff Bases. *Orient. J. Chem.* **2017**, *33*, 165–172. [CrossRef]